Solution Structures of Chromium(VI) Complexes with Glutathione and Model Thiols

ARTICLE *in* INORGANIC CHEMISTRY · FEBRUARY 2004

Impact Factor: 4.76 · DOI: 10.1021/ic034901v · Source: PubMed

2 AUTHORS:

Aviva Levina
University of Sydney
93 PUBLICATIONS **2,531** CITATIONS
SEE PROFILE

Peter A. Lay
University of Sydney
293 PUBLICATIONS **7,740** CITATIONS
SEE PROFILE

Inorg. Chem. **2004**, *43*, 324–335

Solution Structures of Chromium(VI) Complexes with Glutathione and Model Thiols

Aviva Levina and Peter A. Lay*

Centre for Heavy Metals Research and Centre for Structural Biology and Structural Chemistry, School of Chemistry, University of Sydney, Sydney, NSW 2006, Australia

Received July 30, 2003

Chromium(VI) complexes of the most abundant biological reductant, glutathione (γ-Glu-Cys-Gly, **I**), are among the likely initial reactive intermediates formed during the cellular metabolism of carcinogenic and genotoxic Cr(VI). Detailed structural characterization of such complexes in solutions has been performed by a combination of X-ray absorption fine structure (XAFS) and X-ray absorption near-edge structure (XANES) spectroscopies, electrospray mass spectrometry (ESMS), UV–vis spectroscopy, and kinetic studies. The Cr(VI) complexes of two model thiols, *N*-acetyl-2-mercaptoethylamine (**II**) and 4-bromobenzenethiol (**III**), were used for comparison. The Cr(VI)–thiolato complexes were generated quantitatively in weakly acidic aqueous solutions (for **I** and **II**) or in DMF solutions (for **II**) or isolated as a pure solid (for **III**). Contrary to some claims in the literature, no evidence was found for the formation of relatively stable Cr(IV) intermediates during the reactions of Cr(VI) with **I** in acidic aqueous solutions. The Cr(VI) complexes of **I**–**III** exist as tetrahedral $[CrO_3(SR)]^-$ (**IVa**) species in the solid state, in solutions of aprotic solvents such as DMF, or in the gas phase (under ESMS conditions). In aqueous or alcohol solutions, reversible addition of a solvent molecule occurs, with the formation of five-coordinate species, $[CrO_3(SR)L]^-$ (**IVb**, probably of a trigonal bipyramidal structure, L = H_2O or MeOH), with a Cr–L bond length of 1.97(1) Å (determined by XAFS data modeling). Complex **IVb** (L = H_2O) is also formed (in an equilibrium mixture with $[CrO_4]^{2-}$) at the first stage of reduction of Cr(VI) by **I** in neutral aqueous solutions (as shown by global kinetic analysis of time-dependent UV–vis spectra). This is the first observation of a reversible ligand addition reaction in Cr(VI) complexes. The formation of **IVb** (rather than **IVa**, as thought before) during the reactions of Cr(VI) with **I** in aqueous solutions is likely to be important for the reactivity of Cr(VI) in cellular media, including DNA and protein damage and inhibition of protein tyrosine phosphatases.

Introduction

Mechanisms of Cr(VI)-induced genotoxicity and carcinogenicity have been a subject of extensive recent research.[1,2] Glutathione (γ-Glu-Cys-Gly), the most abundant of biological reductants (concentrations in cells can be as high as 10 mM),[3] is directly involved in the cellular metabolism of Cr(VI) compounds.[4] It has been known for decades that the reductions of Cr(VI) to Cr(III) with glutathione or other thiols in aqueous solutions (particularly in weakly acidic media, pH 2−4) proceed through orange-red intermediates (λ_{max} = 420−450 nm), which were assigned by most authors as chromium(VI) thioesters.[5−9] Such species are particularly stable for glutathione compared with simpler thiols, and these are likely to be involved in Cr(VI)-induced DNA damage in cells.[5] Wetterhahn and co-workers[10,11] have proposed, on

* Author to whom correspondence should be addressed. E-mail: p.lay@chem.usyd.edu.au.

(1) Codd, R.; Dillon, C. T.; Levina, A.; Lay, P. A. *Coord. Chem. Rev.* **2001**, *216−217*, 533−577 and references therein.
(2) Levina, A.; Codd, R.; Dillon, C. T.; Lay, P. A. *Prog. Inorg. Chem.* **2003**, *51*, 145−250 and references therein.
(3) Kosower, E. M. In *Glutathione: Metabolism and Function*; Arias, I. M., Jacoby, W. B., Eds.; Raven Press: New York, 1976; pp 1−15.
(4) Ning, J.; Grant, M. H. *Toxicol. in Vitro* **2000**, *14*, 329−335.
(5) Connett, P. H.; Wetterhahn, K. E. *J. Am. Chem. Soc.* **1985**, *107*, 4282−4288.
(6) Connett, P. H.; Wetterhahn, K. E. *J. Am. Chem. Soc.* **1986**, *108*, 1842−1847.
(7) McAuley, A.; Olatunji, M. A. *Can. J. Chem.* **1977**, *55*, 3328−3334.
(8) O'Brien, P.; Wang, G.; Wyatt, P. B. *Polyhedron* **1992**, *11*, 3211−3216.
(9) Perez-Benito, J. F.; Lamrhari, D.; Arias, C. *J. Phys. Chem.* **1994**, *98*, 12621−12629.
(10) Brauer, S. L.; Wetterhahn, K. E. *J. Am. Chem. Soc.* **1991**, *113*, 3001−3007.
(11) Brauer, S. L.; Hneihen, A. S.; McBride, J. S.; Wetterhahn, K. E. *Inorg. Chem.* **1996**, *35*, 373−381.

10.1021/ic034901v CCC: $27.50
Published on Web 12/05/2003

Chart 1. Structures of Thiols Used for Generation of Cr(VI) Complexes

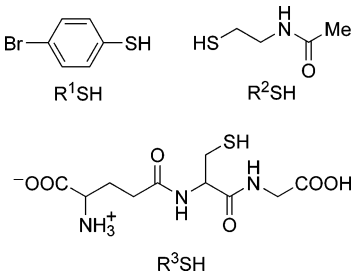

the basis of multinuclear (^{1}H, ^{13}C, and ^{17}O) NMR spectroscopic studies, that glutathione and related thiols form Cr(VI) complexes with a $[CrO_3(SR)]^-$ coordination environment, with monodentate coordination of the ligand (RSH) through the thiolato group. This assignment has been supported by the results of Raman spectroscopy.[12] Mazurek et al.[13,14] have isolated and crystallographically characterized a stable complex, $(Ph_4As)[CrO_3(SR^1)]$ (where R^1SH = 4-bromobenzenethiol, Chart 1), from the reaction of Cr(VI) with R^1SH in DMF solutions. On the other hand, Bose and co-workers[15,16] have argued, on the basis of dynamic magnetic susceptibility measurements, that the intermediate absorbance with $\lambda_{max} \approx 430$ nm during the reactions of Cr(VI) with glutathione at pH 2−4 is due to relatively stable Cr(IV), rather than Cr(VI), intermediates. On the basis of this suggestion, Shi and co-workers[17] claimed the isolation of a stable Cr(IV) complex from the reaction of Cr(VI) with 2 mol equiv of glutathione in aqueous media. The controversy between reports on the formation of Cr(IV)−thiolato[15−17] or Cr(VI)−thiolato[5−12] complexes as the most abundant intermediates of the Cr(VI) reduction by thiols has been resolved herein.

Recently,[18−20] we started to apply a combination of X-ray absorption spectroscopy (XAS),[21] electrospray mass spectrometry (ESMS),[22] and other analytical techniques to the structural characterizations of unstable Cr(VI/V/IV) complexes formed during the reactions of Cr(VI) with biological and model reductants. In the current work, a comparative study of a well-characterized Cr(VI)−thiolato complex, $(Ph_4As)[CrO_3(SR^1)]$,[13,14] and the relatively stable intermediates, formed during the reactions of Cr(VI) with *N*-acetyl-2-mercaptoethylamine (R^2SH in Chart 1) or glutathione (R^3SH in Chart 1), has been performed. The R^2SH ligand models the binding site responsible for the formation of a Cr(V)−R^3SH complex (thiolato and amido donors of the cysteine residue),[20] and is easily soluble both in water and in organic solvents (unlike for R^1SH or R^3SH), which simplifies the studies of Cr(VI)−thiolato complexes formed in aqueous and nonaqueous media. The characterization of the solution structures and chemistry of Cr(VI)−thiolato complexes is important in understanding the following redox chemistry that ultimately leads to Cr-induced cancers.

Experimental Section

Caution! Cr(VI) and As(III) compounds are human carcinogens;[23,24] appropriate precautions should be taken to avoid skin contact and inhalation of solutions and dusts.

Reagents. The following reagents of analytical or higher purity grade were used without further purification: 4-bromobenzenethiol, *N*-acetyl-2-mercaptoethylamine, glycine, and boron nitride (all from Aldrich); glutathione (reduced and oxidized forms) from Sigma; $(Ph_4As)Cl$ from Fluka; $K_2Cr_2O_7$, $Na_2Cr_2O_7 \cdot 2H_2O$, $Na_2CrO_4 \cdot 4H_2O$, CH_3COOH, CF_3COOH, $(NH_4)_2Fe(SO_4)_2 \cdot 6H_2O$, KBr, NaOH, H_2O_2 (aqueous, 30%), and HCl (all from Merck); $(NH_4)_2Cr_2O_7$ from Ajax Chemicals; and *N*-(2-hydroxyethyl)piperazine-*N*′-(2-ethanesulfonic acid) (HEPES) from Research Organics. HPLC grade solvents from Aldrich (purity ≥99.9%) were used as received. Water was purified by the Milli-Q technique. Tetraphenylarsonium (4-bromophenylthiolato)trioxochromate(VI), $(Ph_4As)[CrO_3SR^1]$, was synthesized by a literature method;[13,14] its purity and composition were confirmed by FTIR spectroscopy (Figure S1 in the Supporting Information), elemental analyses (Found: C, 53.3; H, 3.66; S, 4.73; Cr, 7.8. Calcd for $C_{30}H_{24}AsBrCrO_3S$: C, 53.7; H, 3.58; S, 4.78; Cr, 7.8), and magnetic susceptibility measurements ($\mu = 0$ μ_B indicates the absence of Cr(V) or Cr(III) impurities).

Analytical Techniques. All measurements were performed at 22 ± 1 °C (except for some kinetic experiments at 4 or 10 °C), using freshly prepared (within ∼15 min), Ar-saturated solutions. The ultraviolet−visible (UV−vis) spectra were acquired on a Hewlett-Packard HP 8452A diode-array spectrophotometer, and stopped-flow UV−vis spectroscopic measurements were performed using an Applied Photophysics SX-17MV spectrophotometer with a diode-array detector, as described previously.[25,26] In a typical kinetic experiment for the Cr(VI) + R^3SH reaction, 250 time-dependent spectra (logarithmic time base, integration time 2.56 ms, deadtime ∼2 ms, λ = 330−740 nm, resolution ∼1 nm) were collected at 0−1000 s. The absence of a significant influence of UV radiation on the reaction kinetics was verified by comparison of the kinetic curves obtained with the diode-array detector and those acquired at single wavelengths (450 or 630 nm) using a monochromator and a photomultiplier detector.[26] Time-dependent UV−vis spectra were processed with ProKineticist global kinetic analysis software.[27] For studies of the solvent dependencies of the

(12) Meloni, P. A.; Czernuszewicz, R. S. *Vib. Spectrosc.* **1993**, *5*, 205−213.
(13) Mazurek, W.; Fallon, G. D.; Nichols, P. J.; West, B. O. *Polyhedron* **1990**, *5*, 777−779.
(14) Mazurek, W.; Nichols, P. J.; West, B. O. *Polyhedron* **1991**, *10*, 753−762.
(15) Bose, R. N.; Moghaddas, S.; Gelerinter, E. *Inorg. Chem.* **1992**, *31*, 1987−1994.
(16) Moghaddas, S.; Gelerinter, E.; Bose, R. N. *J. Inorg. Biochem.* **1995**, *57*, 135−146.
(17) Liu, K. J.; Shi, X.; Dalal, N. S. *Biochem. Biophys. Res. Commun.* **1997**, *235*, 54−58.
(18) Codd, R.; Levina, A.; Zhang, L.; Hambley, T. W.; Lay, P. A. *Inorg. Chem.* **2000**, *39*, 990−997.
(19) Headlam, H. A.; Weeks, C. L.; Turner, P.; Hambley, T. W.; Lay, P. A. *Inorg. Chem.* **2001**, *40*, 5097−5105.
(20) Levina, A.; Zhang, L.; Lay, P. A. *Inorg. Chem.* **2003**, *42*, 767−784.
(21) Penner-Hahn, J. E. *Coord. Chem. Rev.* **1999**, *190−192*, 1101−1123.
(22) Henderson, W.; Nicholson, B. K.; McCaffrey, L. J. *Polyhedron* **1998**, *17*, 4291−4313.
(23) IARC. *Monographs on the Evaluation of Carcinogenic Risk to Humans. Vol. 49. Chromium, Nickel and Welding*; International Agency for Research on Cancer: Lyon, France, 1990; see also references therein.
(24) Farrell, R. P.; Costa, M. In *Comprehensive Toxicology*; Sipes, I. G., McQueen, C. A., Gandolfi, A. J., Eds.; Pergamon Press: New York, 1997; Vol. 12, pp 225−254 and references therein.
(25) Lay, P. A.; Levina, A. *Inorg. Chem.* **1996**, *35*, 7709−7717.
(26) Levina, A.; Lay, P. A.; Dixon, N. E. *Inorg. Chem.* **2000**, *39*, 385−395.
(27) *Pro-Kineticist*, Version 4.10; Applied Photophysics: Leatherhead, U.K., 1996.

UV−vis spectra of Cr(VI)−thiolato complexes, the spectra were taken at ∼15 s after 100-fold dilution of the stock solution of a Cr(VI) complex with a required solvent; no significant changes in the spectra of a dilute solution occurred for at least 2 min at 22 °C.

The ESMS analyses were performed using a Finnigan LCQ mass spectrometer. Typical experimental settings were as follows: sheath gas (N_2) pressure 60 psi, spray voltage 5.0 kV, capillary temperature 200 °C, capillary voltage 20 V, tube lens offset 20 V, *m*/*z* range 50−2000 (in both positive- and negative-ion modes). These conditions provided optimal sensitivity for most of the observed signals. No major new signals were observed with variations in the spray voltage (4.0−6.0 kV), capillary temperature (150−250 °C), and capillary voltage (5−30 V). Two sample injection methods were used: (i) injection of 5 μL of the sample (in H_2O or *N*,*N*-dimethylformamide (DMF) solution) into a flow of H_2O/CH_3OH (1:1 v/v; flow rate 0.20 mL min^{-1}) and (ii) direct injection of the sample using a syringe drive (flow rate 10 μL min^{-1}). There were no qualitative differences in the spectra obtained from either method, although the former method improved the sensitivity by providing optimal spraying conditions,[28] and allowed faster data acquisition (within ∼30 s) for the reactive Cr(VI)−thiolato complexes. Acquired spectra were the averages of ≥10 scans (scan time 10 ms). Simulations of the isotopic distributions were performed using IsoPro software.[29] The only signals observed in the positive-ion mode were those due to Ph_4As^+ and to the protonated forms of the ligands. No significant signals (in either positive- or negative-ion modes) were observed at *m*/*z* > 1000. All of the results of UV−vis spectroscopic, kinetic, and ESMS studies were reproduced in at least two independent experimental series, using different sets of stock solutions. Typical relative deviations in the results of parallel experiments were <10% (up to 20% for minor ESMS signals). The trends in condition and time dependencies of the spectra remained the same in parallel experiments.

The pH values of the aqueous solutions were measured using a Hanna Instruments HI 9023 ionometer with an HI 1038 glass/Ag/AgCl electrode. EPR spectra (X-band, 22 °C) were acquired on a Bruker EMX specrometer; the spectrometer settings corresponded to those described previously.[20] Fourier transform (FT) IR spectra were acquired in a KBr matrix using the diffuse reflectance technique on a BioRad FTS-40 spectrometer. Magnetic susceptibility was measured on a Sherwood Scientific magnetic susceptibility balance, calibrated with $(NH_4)_2Fe(SO_4)_2{\cdot}6H_2O$. Chromium determination in $(Ph_4As)[CrO_3(SR^1)]$ was performed spectrophotometrically (as $[CrO_4]^{2-}$, $\lambda_{max} = 372$ nm, $\epsilon_{max} = 4.81 \times 10^3$ M^{-1} cm^{-1}), after decomposition of the sample in $NaOH/H_2O_2$ solution.[30] Elemental analyses (C, H, S) were performed by the Australian National University (ANU) Microanalytical Service, using a Carlo Erba 1106 automatic analyzer.

XAS and Data Processing. Chromium K-edge spectra of the Cr(VI)−R^iSH complexes (i = 1−3, Chart 1), as well as that of aqueous Na_2CrO_4 (10 mM, pH 7.0), were recorded at beamline 9-3 at the Stanford Synchrotron Radiation Laboratory (SSRL) or at the Australian National Beamline Facility (ANBF; beamline 20B) at the Photon Factory (Tsukuba, Japan). Conditions for preparation of the samples are listed in Table 1. Experimental settings for both beamlines are listed in Table S1 (Supporting Information). Data collection at low temperature (10 K) minimized photodamage of the samples, improved the signal-to-noise ratio, and maximized the multiple-scattering (MS) contribution to the X-ray absorption fine structure (XAFS) spectrum.[31]

Table 1. Preparation of Samples for XAS

sample	conditions[a]
1[b]	solid $(Ph_4As)[CrO_3(SR^1)]$ mixed with BN (1:1 mass ratio)
2[b,c]	10 mM $(Ph_4As)[CrO_3(SR^1)]$ in DMF, 1 min, 22 °C
3[b]	10 mM $(Ph_4As)[CrO_3(SR^1)]$ in MeOH, 1 min, 22 °C
4[c]	10 mM Cr(VI)[d] + 20 mM R^2SH + 80 mM CH_3COOH in DMF, 1 h, 22 °C
5[c]	10 mM Cr(VI)[e] + 20 mM R^2SH + 80 mM CH_3COOH in H_2O, pH 3.6, 120 s, 4 °C
6[c]	10 mM Cr(VI)[e] + 20 mM R^3SH + 10 mM CF_3COOH in H_2O, pH 2.9, 90 s, 4 °C
7[c]	10 mM Na_2CrO_4 in H_2O, pH 7.0, 1 min, 22 °C

[a] All solutions were snap-frozen in liquid N_2–hexane (1:1) slurry at the specified time and then cooled to 10 K prior to measuring the XAS. [b] Data collected at the ANBF. [c] Data collected at the SSRL. [d] $(NH_4)_2Cr_2O_7$ was used as a source of Cr(VI). [e] $Na_2Cr_2O_7$ was used as a source of Cr(VI).

Averaging, background subtraction, and the calculations of theoretical XAFS spectra were performed using the XFIT software package,[32] including FEFF 4.06[33] and FEFF 6.01[34] algorithms (for single and multiple scattering, respectively), as described previously.[18−20,31] Conditions, restraints, and constraints applied to the XAFS calculations are listed in the Supporting Information. Starting coordinate sets used for MS XAFS calculations were obtained from molecular models generated by HyperChem software.[35] Significantly overdetermined models[36] were used in all calculations (see the Results), and convergence was typically achieved within 100−400 optimization cycles.

The random errors in the estimated XAFS parameters, arising from the noise in the data, were determined by Monte Carlo analysis within the XFIT software.[32]

The following method, combining three known approaches,[32,36,37] has been applied to compare the goodness-of-fit parameters for various models used in the single-scattering (SS) and MS XAFS calculations. An absolute index of the goodness-of-fit,[36] taking the degree of overdeterminacy in the system into account, was calculated for each model:

$$\epsilon_\nu^2 = [1/(N_i - p)](N_i/N)(R/100)^2 \quad (1)$$

where N_i is the number of independent observations, p is the number of fitted parameters, N is the number of data points in k-space, and R (%) is the goodness-of-fit parameter, as defined in the XFIT software.[32] The values of N_i and p in eq 1 were calculated taking into account the applied restraints and constraints.[36] The values of ϵ_ν^2 for two models were considered significantly different when their ratio F exceeded the tabulated value (F-test at 95% confidence interval).[37,38] The numbers of degrees of freedom for each model, used in the F-test, were defined as[37]

$$\nu = N_i - p \quad (2)$$

(28) Cole, R. B. *J. Mass Spectrom.* **2000**, *35*, 763−772.
(29) *IsoPro*, Version 3.0; M. Senko: Sunnyvale, CA, 1998.
(30) Haupt, G. W. *Natl. Bur. Stand. Circ. (U.S.)* **1952**, *48*, 414−423.
(31) (a) Rich, A. M.; Armstrong, R. S.; Ellis, P. J.; Freeman, H. C.; Lay, P. A. *Inorg. Chem.* **1998**, *37*, 5743−5753. (b) Rich, A. M.; Armstrong, R. S.; Ellis, P. J.; Lay, P. A. *J. Am. Chem. Soc.* **1998**, *120*, 10827−10836.
(32) (a) Ellis, P. J.; Freeman, H. C. *J. Synchrotron Radiat.* **1995**, *2*, 190−195. (b) *XFIT for Windows'95*; Australian Synchrotron Research Program: Sydney, Australia, 1996.
(33) Mustre de Leon, J.; Rehr, J. J.; Zabinsky, S. I.; Albers, R. C. *Phys. Rev. B* **1991**, *44*, 4146−4156.
(34) Zabinsky, S. I.; Rehr, J. J.; Ankudinov, A.; Albers, R. C.; Eller, M. J. *Phys. Rev. B* **1995**, *52*, 2995−3009. *Phys. Rev. Lett.* **1992**, *69*, 3397−3400.
(35) *HyperChem*, Version 5.1; Hypercube Inc.: Gainesville, FL, 1996.
(36) Binsted, N.; Strange, R. W.; Hasnain, S. S. *Biochemistry* **1992**, *31*, 12117−12125.

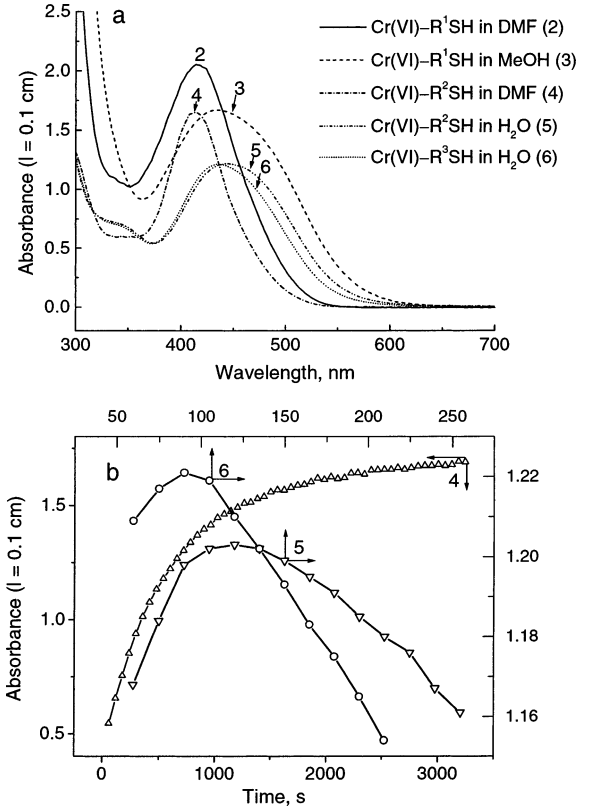

Figure 1. (a) UV−vis spectra of the solutions of Cr(VI)−thiolato complexes, used for XAS. (b) Kinetic curves at 420 nm (4) or at 434 nm (5 and 6) for the formation and decay of Cr(VI)−thiolato complexes. The numbering of the spectra and the kinetic curves corresponds to that given in Table 1.

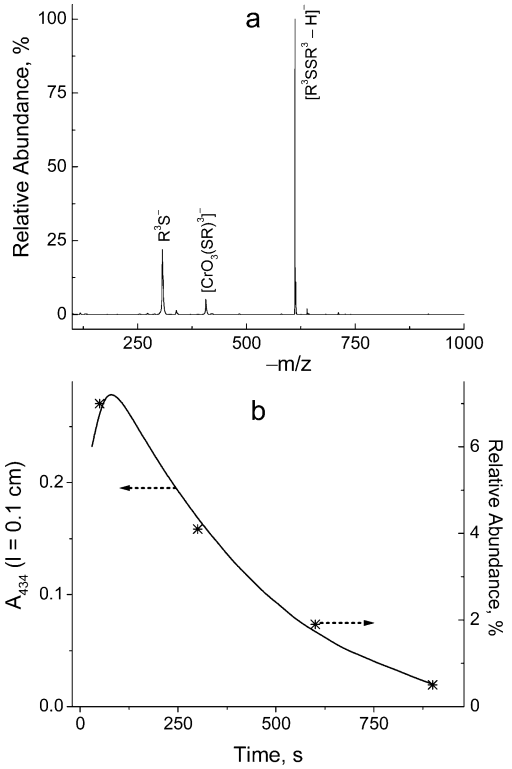

Figure 2. Comparison of ESMS and UV−vis spectroscopic data for the reaction of Cr(VI) (2.0 mM, from $Na_2Cr_2O_7$) with R^3SH (20 mM) in the presence of R^3SSR^3 (50 mM) at pH 2.7 and 22 °C:[15] (a) typical ESMS data for the reaction mixture (at 50 s); (b) solid line, absorbance changes at 434 nm; symbols, changes in relative abundance of the $[CrO_3(SR^3)]^-$ signal vs that of $[R^3SSR^3H]^-$ in ESMS.

Results

Conditions for Quantitative Generation of Cr(VI)−Thiolato Complexes. The conditions used to generate the solutions of Cr(VI) complexes with R^2SH or R^3SH (samples 4−6 in Table 1) were chosen from time-dependent UV−vis spectroscopic studies of the Cr(VI) + R^iSH reactions ($i = 2$ or 3, Chart 1), to provide the maximal intensity and stability of the intermediate absorbance at $\lambda \approx 415$ nm (DMF solutions) or $\lambda \approx 435$ nm (H_2O solutions).[11] The UV−vis spectra of the solutions of Cr(VI)−thiolato complexes (in DMF or H_2O, Figure 1a), used for XAS, were in agreement (within 10% error) with the literature data for such complexes.[11,14] Notably, similar UV−vis spectra were obtained for the two complexes generated in aqueous solutions (samples 5 and 6 in Table 1 and Figure 1a). The UV−vis spectra of the solutions in DMF or MeOH (samples 2−4 in Table 1) did not change (within 1−2%) for at least 2 min at 22 °C. The time points used for snap-freezing the solutions for XAS corresponded to maximal absorbances at 420 nm for sample 4, or 434 nm for samples 5 and 6 (Figure 1b and Table 1). The only significant Cr-containing species (>95%), observed in the studied systems (samples 2−6 in Table 1) by ESMS, were the corresponding $[CrO_3(SR^i)]^-$ complexes (Figures S2 and S3 and Table S2 in the Supporting Information; $i = 1-3$, Chart 1) at these time points. Previously, the ESMS signals of $[CrO_3(SR^3)]^-$ were observed for the Cr(VI) + R^3SH reactions in neutral aqueous solutions.[20] In summary, the solutions used for XAS contained (at the moment of freezing) at least 90−95% Cr(VI)−thiolato complexes (relative to total Cr), according to the ESMS and UV−vis spectroscopic data.

Are Stable Cr(IV) Complexes Formed during the Reduction of Cr(VI) by Glutathione? The ESMS and kinetic results obtained here (Figures 1, S2, and S3) and elsewhere[20] confirm that the absorbance of an intermediate observed at 420−450 nm during the reduction of Cr(VI) with thiols in aqueous solutions is due to Cr(VI)−thiolato complexes.[5−12] Comparative ESMS and kinetic studies of the Cr(VI) + R^3SH reaction have also been performed under the conditions used by Bose and co-workers to generate the purported relatively stable Cr(IV)−R^3SH intermediates.[15,16] Figure 2 shows the results of such a study for the reaction in the presence of excess R^3SSR^3 (oxidized glutathione), used to maintain a constant pH value in the reaction mixture[15] ($[Cr(VI)]_0 = 2.0$ mM, $[R^3SH]_0 = 20$ mM, $[R^3SSR^3] = 50$ mM, pH 2.7, 22 °C). The only Cr-containing species detected in this system by ESMS was $[CrO_3(SR^3)]^-$ ($m/z = -406.6$, Figure 2a and Table S2), and its relative abundance changed concominantly with changes in the intermediate absorbance at $\lambda_{max} = 434$ nm (Figure 2b). The abundance of the $[CrO_3(SR^3)]^-$ signal was measured relative to that of

(37) Kuzmin, A. *EDA: EXAFS Data Analysis Software Package*; Solid State Physics Institute: Riga, Latvia, 1999 (http://www.dragon.lv/exafs).
(38) Neville, A. M.; Kennedy, J. B. *Basic Statistical Methods for Engineers and Scientists*; International Textbook Co.: Scranton, PA, 1966; pp 312−313.

$[R^3SSR^3H]^-$ (as R^3SSR^3 was in a large excess over Cr, its concentration did not change significantly during the reaction). The UV−vis spectrum of the intermediate was not significantly different from that in the absence of excess R^3SSR^3 (e.g., sample 6 in Figure 1a). Similar results were obtained for the Cr(VI) + R^3SH reaction in glycine/HCl buffer ($[Cr(VI)]_0 = 2.0$ mM, $[R^3SH]_0 = 20$ mM, [glycine] = 0.10 M, pH 2.40, 22 °C), where the formation of a relatively stable Cr(IV) intermediate was also suggested from the magnetic measurements.[16]

A reaction under the conditions used by Shi and coworkers[17] to isolate the purported Cr(IV)−R^3SH complex ($[Na_2Cr_2O_7]_0 = 25$ mM, $[R^3SH]_0 = 100$ mM, in H_2O, 2 h at 22 °C) led to a brown-green precipitate, probably a mixture of polymeric Cr(III) complexes, containing traces of Cr(V) and Cr(VI) compounds.[1] No significant ESMS signals could be obtained for this substance due its poor solubility in common solvents, but the filtrate from this reaction (pH 5.5) showed the ESMS signals of $[HCrO_4]^-$ ($m/z = -117.1$),[20] R^3S^-, $[CrO_3(SR^3)]^-$, and $[R^3SSR^3H]^-$ (Table S2). Thus, the ESMS and kinetic studies failed to detect any evidence for the formation of stable Cr(IV) intermediates under the conditions where the formation of such species was previously suggested.[15−17]

Solvent Dependencies of UV−Vis Spectra of the Cr(VI)−Thiolato Complexes. A substantial difference in the UV−vis spectra of Cr(VI)−thiolato complexes in DMF or H_2O solutions (e.g., sample 4 vs sample 5 in Figure 1a) has been observed previously,[11] but no explanation for this phenomenon was given. The spectra of $(Ph_4As)[CrO_3(SR^1)]$ (0.10 mM, prepared from a 10 mM stock solution in DMF) in a range of aprotic solvents were similar (Table S3 in the Supporting Information). By contrast, the spectra of this compound in protolytic solvents (H_2O, MeOH, or EtOH) were distinguished with significantly red-shifted, lower, and broader absorbance bands (Figure 3a and Table S3); these changes corresponded to a color change from yellow to orange. The spectral changes were complete within the deadtime of the stopped-flow spectrometer (<2 ms) at 10 or 22 °C.

The spectra of $(Ph_4As)[CrO_3(SR^1)]$ in H_2O/DMF or MeOH/DMF mixtures showed complex dependencies on the solvent compositions with no single isosbestic points (Figure S4 in the Supporting Information). The spectrum of $(Ph_4As)[CrO_3(SR^1)]$ (0.10 mM) in a mixture of H_2O (90 vol %) and DMF (10 vol %) was not significantly affected by addition of $HClO_4$ (up to 10 mM), while addition of NaOH (≥0.1 mM) caused rapid (<15 s) decomposition of the complex with the formation of $[CrO_4]^{2-}$ ($\epsilon_{max} = 4.81 \times 10^3$ M^{-1} cm^{-1} at $\lambda_{max} = 372$ nm).[30]

When an aqueous solution of the Cr(VI)−R^3SH complex ([Cr] = 10 mM, generated according to condition 6 in Table 1) was diluted 100-fold with H_2O, MeOH, or DMF, the UV−vis spectra of the dilute solutions (Figure 3b and Table S3) were similar to those of $(Ph_4As)[CrO_3(SR^1)]$ in the corresponding solvents (Figure 3a). When stock solutions of the Cr(VI)−R^2SH complex ([Cr] = 10 mM), generated in either DMF or H_2O (condition 4 or 5 in Table 1, respectively) were diluted 100-fold with H_2O, MeOH, or DMF, the resultant spectra were determined by the diluting solvent, rather than by the solvent in which the complex was generated (Table S3 and Figure S5 in the Supporting Information). In summary, the solvent dependencies of UV−vis spectra of the Cr(VI)−thiolato complexes (Figures 1, 3, S4, and S5 and Table S3) point to reversible structural changes in the complexes in protolytic solvents (such as H_2O, MeOH, or EtOH).

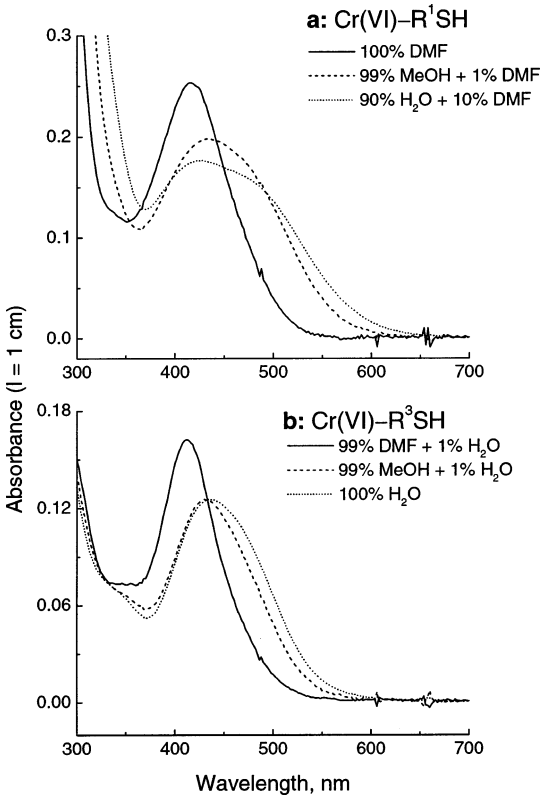

Figure 3. UV−vis spectra of Cr(VI)−thiolato complexes in various solvents ([Cr] = 0.10 mM; solvent compositions are given in volume percent). Stock solutions ([Cr] = 10 mM) of (a) $(Ph_4As)[CrO_3(SR^1)]$ in DMF or (b) the Cr(VI)−R^3SH complex (generated according to condition 6 in Table 1) were diluted 100-fold with the corresponding solvent (DMF, MeOH, or H_2O) ~15 s (22 °C) before acquisition of the spectra.

UV−Vis Spectra of the Cr(VI)−R^3SH Complex in Neutral Aqueous Solutions. Numerous kinetic studies of the Cr(VI) reactions with R^3SH and other thiols in neutral aqueous solutions[1,5,6,8,9,20,25] have shown that the Cr(VI)−thiolato complexes are formed under these conditions as unstable intermediates that coexist in the reaction mixtures with $[CrO_4]^{2-}$, Cr(V), and Cr(III) species. Application of global kinetic analysis made calculations of UV−vis spectra of such intermediates possible.[25,26] In this work, the kinetics of the Cr(VI) + R^3SH reactions were studied by following the time-dependent spectral changes ($\lambda = 330-740$ nm) at $[Cr(VI)]_0 = 0.05-0.20$ mM and $[R^3SH]_0 = 5-20$ mM in HEPES buffer (0.10 M, pH 7.40) at 22.0 °C. The use of a large excess of R^3SH over Cr(VI) (50−200 mol equiv) allowed the kinetics to be evaluated using a reaction scheme that involved only pseudo-first-order steps (Scheme 1).[25] HEPES buffer was chosen because of its known minimal effects on the kinetics of reactions involving high oxidation

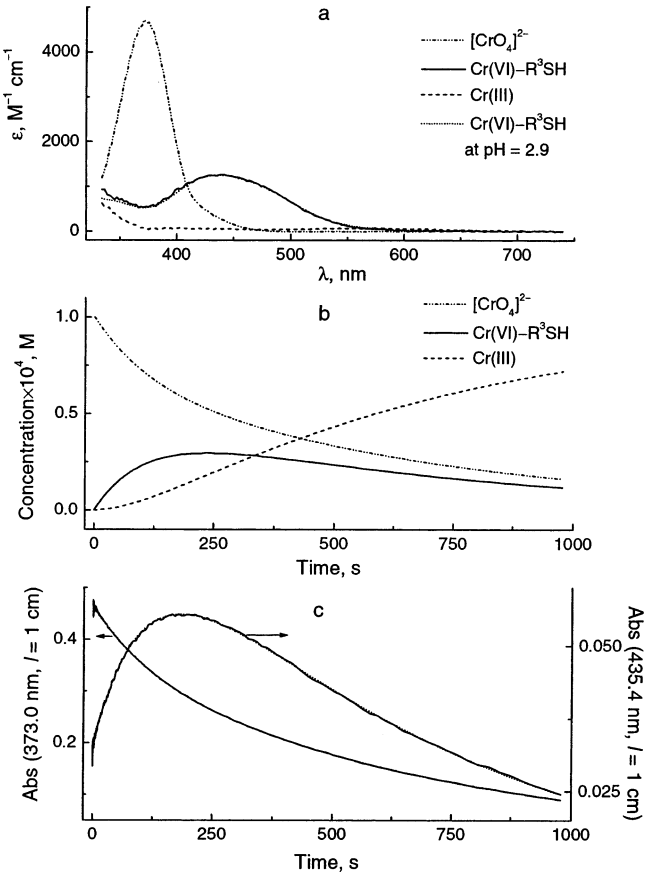

Figure 4. Typical results of global kinetic analysis for the Cr(VI) + R^3SH reaction in neutral aqueous solution ($[Cr(VI)]_0 = 0.10$ mM, $[R^3SH] =$ 10 mM, 0.10 M HEPES buffer, pH 7.4, Ar-saturated solution, 22.0 °C): calculated spectra (a) and kinetic curves (b) for the reacting species, and typical observed (solid lines) and calculated (dotted lines) kinetic curves (c). The kinetic analysis was performed according to Scheme 1,[9] with optimized values of the rate constants (Table S4) of $k_1 = 3.8 \times 10^{-3}$ s^{-1}, $k_{-1} = 3.2 \times 10^{-3}$ s^{-1}, and $k_2 = 3.5 \times 10^{-3}$ s^{-1}.

Scheme 1. Kinetic Scheme Applied to the Reactions of Cr(VI) with a Large Excess of R^3SH at pH 7.40

$$[CrO_4]^{2-} + R^3SH \underset{k_{-1}}{\overset{k_1}{\rightleftharpoons}} Cr(VI)\text{–}R^3SH \xrightarrow{k_2} Cr(III)$$

states of Cr,[26] and on the speciation of intermediates in such reactions.[39] All of the kinetic data were successfully fitted with a sequence of reversible formation and irreversible decomposition reactions of a Cr(VI)−R^3SH intermediate (Scheme 1).[9] No detectable levels of Cr(V) intermediates (by EPR spectroscopy) were formed under the studied conditions.

Typical results of kinetic analyses are shown in Figure 4, and a list of observed rate constants at different reagent concentrations is given in Table S4 (Supporting Information). The values of k_1 (Scheme 1) were linearly dependent on $[R^3SH]_0$, while the values of k_{-1} and k_2 were independent of $[R^3SH]_0$ (Table S4). All the observed rate constants (Scheme 1) were independent of $[Cr(VI)]_0$ (Table S4). Calculated spectra of the initial compound and the final product (Figure 4a) correspond to those of $[CrO_4]^{2-}$ and the Cr(III)−R^3SH−R^3SSR[3] complexes, respectively (R^3SH and its oxidized form, R^3SSR[3], are colorless within the studied wavelength range).[20,40]

(39) Zhang, L.; Lay, P. A. *Aust. J. Chem.* **2000**, *53*, 7−13.

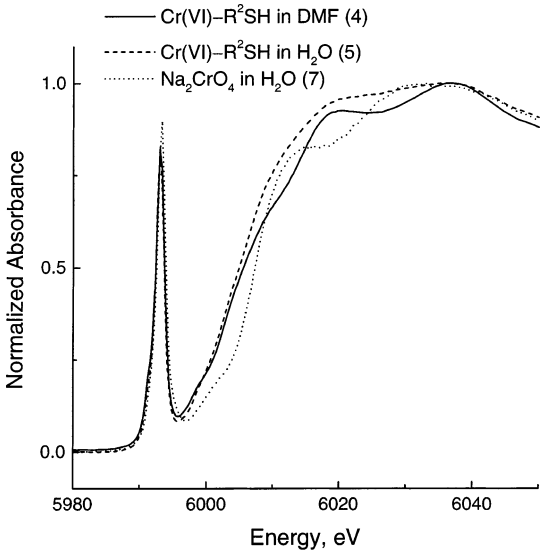

Figure 5. Typical XANES spectra of Cr(VI) complexes (10 K), collected at the SSRL (see also Figure S6 in the Supporting Information). The numbers in parentheses correspond to the conditions in Table 1.

Table 2. XANES Spectral Characteristics of Cr(VI) Complexes at 10 K

sample[a]	edge energy,[d] eV	preedge energy, eV	preedge intensity, %	edge shift,[e] eV	preedge decrease,[e] %
1[b]	6006.4	5992.9	71.0	0	0
2[c]	6005.9	5993.0	85.9	−0.3	5
2[b]	6005.6	5993.1	61.1	0	0
3[b]	6005.2	5993.0	60.9	0	0
4[c]	6005.6	5993.0	82.0	−0.6	15
5[c]	6005.1	5993.0	83.3	−0.2	7
6[c]	6005.0	5993.0	83.0	−0.4	7
7[c]	6007.3	5993.4	90.3	−0.4	10

[a] The numbering of the samples corresponds to Table 1. [b] Data collected at the ANBF. [c] Data collected at the SSRL. [d] Measured at 50% of the edge jump. [e] Comparison of XANES spectra for the first and second scans at the same spot (typical examples are given in Figure S6e,f, Supporting Information).

The calculated spectrum of the intermediate (Cr(VI)−R^3SH, Figure 4a) corresponded to that of the Cr(VI)−R^3SH complex, generated at pH 2.9 (condition 6 in Table 1). Small deviations (at $\lambda < 400$ nm) of the intermediate spectrum at pH 7.4 from that of the Cr(VI)−R^3SH complex at pH 2.9 (Figure 4a) are probably due to errors in the kinetic analysis caused by the presence of an excess of highly absorbing $[CrO_4]^{2-}$ (Figure 4a,b). Calculated spectra of the reacting species were the same (within 5% experimental error) in all the kinetic experiments (Table S2). Thus, the same Cr(VI)−R^3SH species are likely to be formed during the Cr(VI) + R^3SH reactions at pH 2.9 (Table 1 and Figures 1 and 3b) and pH 7.4 (Figure 4).

X-ray Absorption Near-Edge Structure (XANES) Spectra of Cr(VI)−Thiolato Complexes. The XANES spectra of the Cr(VI)−thiolato complexes and $[CrO_4]^{2-}$ are shown in Figures 5 and S6 (Supporting Information), and the numeric data are summarized in Table 2. All of the spectra possessed sharp and intense preedge peaks due to the 1s → 3d electronic transition, characteristic for Cr(VI)−oxo com-

(40) Brasch, N. E.; Buckingham, D. A.; Evans, A. B.; Clark, C. R. *J. Am. Chem. Soc.* **1996**, *118*, 7969−7980.

plexes (Figures 5 and S6 and Table 2).[41] A comparison of XANES spectra for two identical samples (condition 2 in Table 1), collected at the SSRL or at the ANBF, revealed a significantly lower and wider preedge peak, as well as a slight change in the edge shape, for the latter spectrum (Figure S6a). Similar differences were observed between the spectrum of solid $(Ph_4As)[CrO_3(SR^1)]$ and that of a DMF solution of the same complex (Figure S6b; both of the spectra were acquired at the ANBF). These changes in XANES spectra were probably caused by the differences in the signal-to-noise ratio, as well as the lower resolution of the monochromator crystal at the ANBF compared with that at the SSRL. The spectrum of the Cr(VI)−R^2SH complex in H_2O was markedly different from that of the same complex in DMF (in the 6005−6035 eV area, Figure 5). Similar but less pronounced differences were observed for the spectra of the Cr(VI)−R^1SH complex in DMF or MeOH (Figure S6b). On the other hand, the spectra of the Cr(VI)−R^1SH and Cr(VI)−R^2SH complexes in DMF were similar, as were those of the Cr(VI)−R^2SH and Cr(VI)−R^3SH complexes in H_2O (Figure S6c,d). In summary, the shapes of the XANES spectra of the Cr(VI)−thiolato complexes were determined by the nature of the solvent rather than the nature of the ligand. The spectrum of aqueous $[CrO_4]^{2-}$ was distinguished from those of the Cr(VI)−thiolato complexes by a significant shift of the edge position to higher energies, and by changes in the general edge structure (Figure 5 and Table 2).

Replicate scans at the same spot for the frozen solutions of Cr(VI) complexes (spectra acquired using a focused beam at the SSRL) revealed slight shifts in the edge energies to lower values and decreases in the intensities of the preedge peaks. Such changes are characteristic for photoreduction of the Cr(VI) complexes (probably leading to Cr(III) species).[31,42] On the other hand, no significant changes in the XANES spectra upon repeat scans at the same spot were observed for the solid-state or solution spectra of $(Ph_4As)[CrO_3(SR^1)]$, acquired using an unfocused beam at the ANBF. Typical examples of replicate XANES scans at the same spot (ANBF or SSRL data) are shown in Figure S6e,f, and the energy values of edge and preedge transitions for all samples are listed in Table 2. For the data collected at the SSRL, only the first scans at each spot were used for the XAFS analyses.

SS Modeling of XAFS Spectra. Detailed results of SS XAFS analyses for the first coordination shells of Cr(VI) complexes (samples 1−7 in Table 1) are listed in Table S5 (Supporting Information). Experimental and calculated XAFS spectra for all the samples (including the use of four- and five-coordinate models), as well as the applied window functions, are shown in Figures S7−S14 (Supporting Information). A summary of the goodness-of-fit parameters for SS XAFS calculations is given in Table 3.

Good fits ($R = 13-18\%$)[32,36] were obtained for solid $(Ph_4As)[CrO_3(SR^1)]$ and for DMF solutions of the Cr(VI) complexes with R^1SH or R^2SH (samples 1, 2, and 4 in Tables 1 and 3), using a two-shell, four-coordinate model (3Cr═O + 1Cr−S, model A in Table S5). The optimized values of Cr−ligand bond lengths (1.61−1.62 Å for Cr═O and 2.26−2.27 Å for Cr−S, Table S5) agreed with those found in the crystal structure of $(Ph_4As)[CrO_3(SR^1)]$ (1.61(1) and 2.263(7) Å, respectively).[13] By contrast, applications of the four-coordinate model A to the XAFS spectra of aqueous solutions of the Cr(VI) complexes with R^2SH or R^3SH (samples 5 and 6 in Tables 1 and 3) led to relatively poor fits ($R \approx 20\%$, Table 3) and to oscillating patterns in the fit residues (Figures S12 and S13), which point to the presence of at least one more scatterer in the first coordination shell of Cr.[21] Addition of one Cr−O/N bond (model B in Table S5) led to statistically significant improvements of the fits for samples 5 and 6 (Table 3).[37,38] The optimized Cr−O/N bond lengths for samples 5 and 6 were 1.97 Å (Table S5), and the Debye−Waller factors for these bonds (0.0010−0.0024 Å^2, Table S5) were within the physically reasonable range for the first coordination shell.[31,32] Application of a model with a varied number of Cr−O/N bonds (3Cr═O + 1Cr−S + *n*Cr−O/N, model C in Table S5) for samples 5 and 6 did not lead to significant improvements of the fits compared with that of model B, and the optimized *n* values were close to 1.0 (Table S5).

Application of model B to the XAFS spectrum of the Cr(VI)−R^1SH complex in MeOH solution (sample 3 in Tables 1 and 3) led to a pronounced improvement of the fit compared with that of model A ($R = 7.7\%$ vs 13.6%, Table S5), although this did not meet the criteria of statistical significance.[38] Application of model C to this system led to a significant improvement of the fit compared with that of model A, and to the optimized number of Cr−O/N bonds $n = 0.77 \pm 0.12$ (Tables 3 and S5). The optimized Cr−O/N

Table 3. Summary of Goodness-of-Fit Parameters in the Optimized SS XAFS Models of the First Coordination Shells of Cr(VI) Complexes at 10 K[a]

			four-coordinate[f]		five-coordinate[g]	
sample[b]	solvent	ligand[e]	R,[h] %	$\epsilon_\nu^2 \times 10^4$ [i]	R,[h] %	$\epsilon_\nu^2 \times 10^4$ [i]
1[c]		R^1SH	18.2	1.65	13.7	1.10
2[d]	DMF	R^1SH	13.0	1.20	10.4	0.74
2[c]	DMF	R^1SH	16.9	1.73	14.5	1.28
3[c]	MeOH	R^1SH	13.6	1.12	6.7[j]	0.37[j,k]
4[d]	DMF	R^2SH	17.0	1.44	15.1	1.34
5[d]	H_2O	R^2SH	20.3	2.09	9.4	0.58[k]
6[d]	H_2O	R^3SH	19.7	2.13	7.1	0.33[k]
7[d]	H_2O		11.8[l]	0.85[l]	11.5[m]	1.06[m]

[a] Detailed descriptions of the SS XAFS models are given in Table S5, Supporting Information, and typical experimental and calculated XAFS spectra are shown in Figures S7−S14. [b] The numbering of the samples corresponds to Table 1. [c] Data collected at the ANBF. [d] Data collected at the SSRL. [e] Chart 1. [f] A two-shell, four-coordinate model: 3Cr═O + 1Cr−S. [g] A three-shell, five-coordinate model: 3Cr═O + 1Cr−S + 1Cr−O/N. [h] Goodness-of-fit parameter.[32] [i] Absolute index of the goodness-of-fit, according to eq 1.[36] Decreases in the values of R and ϵ_ν^2 correspond to improvements in the fits. [j] A three-shell model with varied coordination number: 3Cr═O + 1Cr−S + *n*Cr−O/N ($n = 0.77$ for the optimized model, Table S5). [k] A statistically significant improvement in the ϵ_ν^2 parameter compared with that of the four-coordinate model (according to Fisher's criteria with a 95% confidence level).[37,38] [l] A one-shell, four-coordinate model: 4Cr═O. [m] A two-shell, five-coordinate model: 4Cr═O + 1Cr−O/N.

(41) Bajt, S.; Clark, S. B.; Sutton, R.; Rivers, M. L.; Smith, J. V. *Anal. Chem.* **1993**, *65*, 1800−1804.
(42) Levina, A.; Codd, R.; Hambley, T. W.; Foran, G. J.; Maschmeyer, T.; Masters, A. F.; Lay, P. A. *Inorg. Chem.*, accepted for publication.

Chart 2. Models Applied in MS XAFS Calculations for Sample 6 (Table 1)[a]

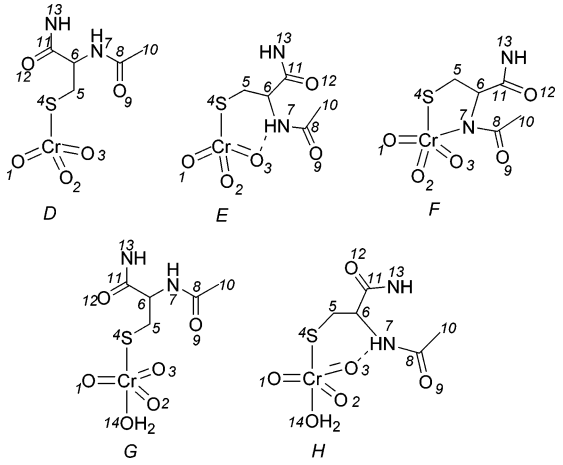

[a] The numbering of the atoms used in the MS XAFS models (Tables S6−S8 in the Supporting Information) is shown in italics.

bond length and the Debye−Waller factor (1.97 and 0.0033 Å^2, respectively, Table S5) for sample 3 (model C) were close to the corresponding values for aqueous solutions (samples 5 and 6, model B). These results suggest that solutions of the Cr(VI)−R^{1}SH complex in MeOH contain a mixture of four- and five-coordinate species.

Application of models B and C to samples 1, 2, and 4 (solid state or DMF solutions, Tables 1 and 3) did not lead to statistically significant improvements of the fits compared with that of model A, although the *R* values did decrease due to increases in the number of fitted parameters (Tables 3 and S5).[36,37] In most of the fits for these samples, using model B or C, the optimized values of Debye−Waller factors (σ^2) of the Cr−O/N bonds were unreasonably high for the first coordination shell (>0.01 Å^2, Table S5).[32] Inclusion of a Cr−O/N bond also did not improve the SS XAFS fit for aqueous $[CrO_4]^{2-}$ (sample 7 in Tables 1, 3, and S5).

Taken together, the results of SS XAFS modeling (Tables 3 and S5 and Figures S7−S14) suggest that the changes in UV−vis and XANES spectra of aqueous and methanolic solutions of Cr(VI)−thiolato complexes, compared with DMF solutions (Figures 1, 3, 5, and S4−S6), are due to the binding of an additional O/N-donor ligand to the four-coordinate $[CrO_3(SR^i)]^-$ complexes (i = 1−3).

MS Modeling of XAFS Spectra. A detailed analysis of XAFS spectra, using an MS approach, was performed for an aqueous solution of the Cr(VI)−R^{3}SH complex (sample 6 in Table 1), in an attempt to clarify the nature of the additional ligand and the structure of the five-coordinate complex. The models used in MS XAFS fits (D−H in Chart 2) included all the non-hydrogen atoms that are likely to be found within 5 Å of the Cr center.[20,31] Conditions, restraints, and constraints, applied to the MS XAFS calculations, parameters of the optimized MS XAFS models, and the most significant scattering paths to the calculated XAFS spectra are listed in Tables S6−S8, Supporting Information. In all the MS XAFS calculations, bond lengths and angles in the R^{3}S$^-$ ligand were restrained (within 0.05 Å and 5°) to those found in the crystal structure of R^{3}SH.[43] The Cr−ligand bond lengths were unrestrained in all calculations. A summary of goodness-of-fit parameters for all the MS XAFS models (Chart 2) is given in Table 4. Typical experimental and calculated XAFS spectra (for model G in Chart 2 and Table 4), as well as the applied window functions, are shown in Figure 6.

Table 4. Summary of Goodness-of-Fit Parameters in the Optimized Fits to the MS XAFS Models of the Aqueous Cr(VI)−R^{3}SH Complex at 10 K[a]

model[b]	*R*,[e] %	$\epsilon_\nu^2 \times 10^4$ [f]	model[b]	*R*,[e] %	$\epsilon_\nu^2 \times 10^4$ [f]
D[c]	20.6	6.2	G[c]	9.5	1.7[g]
D[d]	20.2	6.6	G[d]	8.5	1.6[g]
E[c]	20.7	6.5	H[c]	9.7	1.9[g]
E[d]	20.5	7.6	H[d]	8.4	1.9[g]
F[d]	7.5	0.89[g]			

[a] Sample 6 in Table 1, data collected at the SSRL. Details of the MS XAFS analyses are given in Tables S4−S6, Supporting Information. [b] Designations of the models (D−H) correspond to Chart 2. [c] Bond angles between the ligands were restrained (±10°, Table S7) during the optimizations. [d] Bond angles between the ligands were unrestrained. [e] Goodness-of-fit parameter.[32] [f] Absolute index of the goodness-of-fit, according to eq 1.[36] Decreases in the values of *R* and ϵ_ν^2 correspond to improvements in the fits. [g] A statistically significant improvement in the ϵ_ν^2 parameter compared with that of model D (according to Fisher's criteria with a 95% confidence level).[37,38]

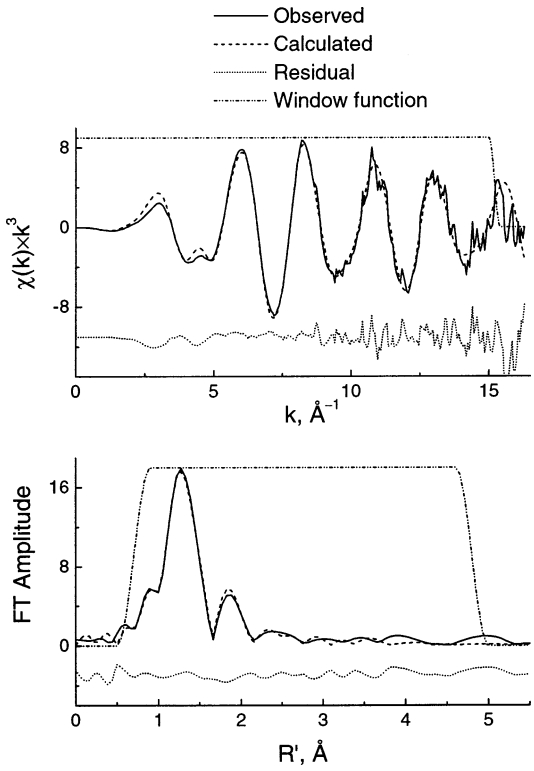

Figure 6. Experimental and calculated (MS, model G in Chart 1 and Table 4) XAFS spectra of the aqueous Cr(VI)−R^{3}SH complex at 10 K (sample 6 in Table 1).

In agreement with the results of SS XAFS analyses, application of tetrahedral models (D and E in Chart 2) to the XAFS spectrum of sample 6 led to poor fits (R > 20%, Table 4). In the initial calculations using models D and E, bond angles between the ligands were restrained to those expected for a tetrahedral structure (110 ± 10°, Table S7).

(43) Wright, W. B. *Acta Crystallogr.* **1958**, *11*, 632−642.

Subsequently, these restraints were released (models D′ and E′ in Tables 4 and S7), which led to significant distortions from the tetrahedral structure (the optimized values of the bond angles are listed in Table S7). Although the *R* values for models D′ and E′ were marginally lower than those for models D and E, the ϵ_ν^2 values for the former models were higher, due to the decrease in the number of degrees of freedom (Table 4).[36,37] Thus, release of the restraints on bond angles between the ligands did not lead to improvements in the fits for models D and E (Chart 2). Model E is distinguished from model D by the presence of a hydrogen bond between an oxo group and an amido group of the R^3S^- ligand (Chart 2). The optimized distances between the O3 and N7 atoms were 4.19 Å for model D and 2.85 Å for model E (Table S7), the latter value is typical for a weak hydrogen bond.[44] This conformational difference between models D and E (or D′ and E′) did not affect the goodness-of-fit parameters (Table 4).

Model F (Chart 2) involved the coordination of Cr(VI) to the thiolato and amido donors of the cysteine residue, similar to that observed in a Cr(V)−R^3SH complex[20] (no restraints were applied to the bond angles between the ligands). Application of model F led to a dramatic improvement in goodness-of-fit parameters compared with that of the four-coordinate models (Table 4), but some of the σ^2 values in the optimized model reached the highest or lowest limits set in the optimization (0.02 Å^2 for C5 and 0.0005 Å^2 for C7, Chart 2 and Table S7). Application of a five-coordinate model involving the coordination of an aqua ligand (model G in Chart 2 and Table 4) led to statistically significant improvements of the fit compared with that of the four-coordinate models (D and E in Table 4), and all the optimized σ^2 values for this model were within a physically reasonable range (0.0008−0.008 Å^2, Table S7). Application of a five-coordinate model including a hydrogen bond (H in Chart 2) did not lead to any improvement of the fit compared with that of model G (Table 4), and some of the σ^2 values for the former model were significantly increased (Table S7). The optimized O3−N7 distances (Chart 2) were 3.63 and 2.93 Å for models G and H, respectively (Table S7). In the initial calculations using models G and H, bond angles between the ligands were restrained (within 10°) to those expected for a trigonal bipyramidal structure with oxo groups in equatorial positions (Table S7).[45] Release of these restraints (models G′ and H′ in Tables 4 and S7) caused significant distortions from the trigonal bipyramidal structure (Table S7), but did not lead to improvements in the fits (Table 4). The optimized Cr−ligand bond lengths for the MS models corresponded (within 0.01 Å experimental error)[32] to those found by SS XAFS analyses (see above).

In summary, the results of MS XAFS analyses for the Cr(VI)−R^3SH complex in aqueous media (sample 6 in Table 1) support the formation of an aquated complex, $[CrO_3(SR^3)(OH_2)]^-$, probably of trigonal bipyramidal structure (model G in Chart 2).[45] Formation of a chelate complex (model F in Chart 2) is less likely, due to the physically unreasonable σ^2 values for the C5 and N7 atoms (Chart 2 and Table S7). The MS XAFS analyses did not give a preference to a three-dimensional structure in which the amide was hydrogen-bonded or not (e.g., G, G′, H, or H′ in Tables 4 and S7), due to relatively small contributions of the atoms beyond the first coordination shell to the XAFS spectrum (Figures 6 and S13 and Table S8).

Discussion

The UV−vis spectra at 22 °C (Figures 1, 3, S4, and S5 and Table S3) and the XAS results at 10 K (Tables 2−4 and S3−S6 and Figure 5) point to a reversible addition of a solvent ligand to the first coordination shells of the $[CrO_3(SR^i)]^-$ complexes (i = 1−3, Chart 1) in aqueous or alcohol solutions. The validity of the XAS data is supported by similar results obtained from several independent samples in either DMF or H_2O solutions (Tables 2−4 and Figures 5 and S6). The optimized values of the Cr−L (L = H_2O or MeOH) bond lengths (1.96−1.97 Å, Tables S5 and S7) were close to those found in the crystallographically characterized $[Cr^{III}(OH_2)_6]^{3+}$ complex (1.96 Å),[46] or in the $[Cr^{VI}O(O_2)_2(OH_2)]$ complex, characterized by XAFS spectroscopy in aqueous solutions (1.93 Å).[47]

Photodecomposition of the samples (Table 2 and Figure S5e,f) did not significantly affect the XAFS data analyses, since consistent results were obtained for the samples with various degrees of decomposition (Table 2). Previously, higher degrees of photoreduction (edge shifts by −0.7 to −1.0 eV in the second scan at the same spot) were observed in the XAS of Cr(V/IV)−2-hydroxycarboxylato complexes in frozen solutions (10 K), using a focused X-ray beam.[42] Nevertheless, the structure determinations of the Cr(V/IV) complexes from XAFS data were not compromized when the scans affected by photodamage were rejected.[42]

The increase in coordination numbers for the Cr(VI) complexes of R^2SH or R^3SH in aqueous solutions, revealed by SS XAFS modeling (Table 3), could also be explained by the formation of chelate complexes with thiolato and amido moieties of the ligands (e.g., model F in Chart 2), since XAFS calculations do not distinguish between O- and N-scatterers.[21,31,32] This coordination mode was previously established (on the basis of the results of XAS and ESMS studies) for the $Na_3[Cr^VO(LH_2)_2]$ complex (where LH_5 = R^3SH), isolated from the reaction of Cr(VI) with excess R^3SH in neutral aqueous media.[20] However, the possibility of such chelation for the Cr(VI)−R^iSH complexes (i = 2 or 3) is essentially ruled out by the results of MS XAFS analyses (see above), as well as by the following considerations. Solvent-dependent UV−vis spectral changes were similar for the Cr(VI) complexes of R^1SH (where the possibility of chelation was excluded), and those of R^2SH or R^3SH (Figures

(44) Lii, J.-H. In *Encyclopedia of Computational Chemistry*; Schleyer, P. v. R., Ed.; John Wiley & Sons: Chichester, U.K., 1998; Vol. 2, pp 1271−1283.
(45) Kepert, D. L. In *Comprehensive Coordination Chemistry*; Wilkinson, G., Gillard, R. D., McCleverty, J. A., Eds.; Pergamon Press: Oxford, U.K., 1987; Vol. 1, pp 32−108.
(46) Lazar, D.; Ribar, B.; Divjakovic, V.; Meszaros, C. *Acta Crystallogr., Sect. C: Cryst. Struct. Commun.* **1991**, *C47*, 1060−1062.
(47) Inada, Y.; Funahashi, S. *Z. Naturforsch., B* **1997**, *52*, 711−718.

3 and S5). An increase in the coordination number of the Cr(VI)−R^1SH complex in MeOH solution compared with those in DMF solution or in the solid state was revealed from XANES spectra (Figure 5) and from SS XAFS analyses (Tables 3 and S5). UV−vis spectra of the Cr(VI)−R^3SH complex were practically identical in aqueous solutions at pH 2.9 or 7.4 (Figure 4), while the formation of a chelate involving a deprotonated amido group (model F in Chart 2) is expected to be favored at the higher pH value. Finally, unlike for the Cr(V)−R^3SH complex,[20] no signals of the chelate species ($[CrO_3(SR^iH)]^{2-}$, $i = 2$ or 3) were observed by ESMS (Figures S2 and S3 and Table S2). Nevertheless, unstable Cr(VI) chelate complexes can be formed as steady-state intermediates during the reduction of Cr(VI) with R^3-SH or related thiols in neutral aqueous solutions.[25]

Coordination of an aqua ligand *trans* to the thiolato group in the $[CrO_3(SR^i)(OH_2)]^-$ complexes ($i = 1-3$, similar to model G in Chart 2) is likely to be energetically favorable compared with *cis*-binding of the thiolato and amido donors in chelate species (model F in Chart 2), due to electrostatic and steric repulsions of the three oxo groups, which tend to occupy equatorial positions in five-coordinate complexes.[45] The proposed trigonal bipyramidal structure of the $[CrO_3(SR^i)(OH_2)]^-$ complexes, similar to model G in Chart 2, is supported (though not directly confirmed) by the results of MS XAFS modeling for the Cr(VI)−R^3SH complex (Tables 4 and S7). The intensities of preedge absorbances in XANES spectra for the samples in either DMF or H_2O solutions did not change significantly (for the spectra with similar signal-to-noise levels, taken at the same X-ray source, Figure 5 and Table 2), due to the absence of significant symmetry changes between the four- and five-coordinate complexes (with $\sim C_{3v}$ symmetry).

No signals that could be attributed to $[CrO_3(SR^i)(OH_2)]^-$ species were observed in aqueous solutions of Cr(VI)−thiolato complexes by ESMS (Figures 2 and S2), in agreement with the commonly observed loss of H_2O ligands from the coordination spheres of Cr complexes during their transfer into the gas phase under ESMS conditions.[48−50] The proposed structure of aqueous Cr(VI)−thiolato complexes is not in conflict with the results of NMR- and Raman-spectroscopic studies, where only thiolato donors were deduced to be bound to Cr(VI) along with the three oxo ligands.[10−12] The absence of evidence for H_2O binding in ^{17}O NMR spectra of the Cr(VI)−R^3SH complex[10,11] can be explained by fast aqua exchange of the relatively weakly coordinated H_2O with the bulk solvent, in agreement with the kinetically labile nature of Cr(VI) complexes[51] (the fast H_2O exchange in the Cr(VI)−thiolato complexes was confirmed by stopped-flow spectrophotometry; see the Results). The absence of a single isosbestic point in a series of UV−vis spectra of Cr(VI)−R^1SH complexes in mixed H_2O/DMF or MeOH/DMF solvents (Figure S4) is probably due to the influence of the changing solvent properties (dielectric constants and specific solvation effects from the coordinated ligands), as well as the changing $[CrO_3(SR^1)]^-/[CrO_3(SR^1)L]^-$ ratios ($L = H_2O$ or MeOH). This feature complicates the calculations of equilibrium constants. The following observations are consistent with a quantitative (at least 90−95% of the total Cr) formation of $[CrO_3(SR^i)(OH_2)]^-$ ($i = 2$ or 3) under conditions 5 or 6 in Table 1: (i) the results of SS XAFS fits in which the coordination numbers were allowed to vary, pointing to the binding of another ligand to the four-coordinate Cr(VI)−R^iSH complexes (model C in Table S3), and (ii) the absence of significant differences in the UV−vis spectra of the Cr(VI)−R^iSH complexes in aqueous solutions at [Cr] = 10 or 0.10 mM (Figures 1, 3b, and S5), which rules out the formation of oxo-bridged dinuclear species. On the other hand, the results of SS XAFS analyses (Tables 3 and S5) and XANES spectra (Figures 5 and S6) point to the existence of an equilibrium mixture of the $[CrO_3(SR^1)]^-$ and $[CrO_3(SR^1)(OHMe)]^-$ species in the solutions of the Cr(V)−R^1SH complex in MeOH (condition 3 in Table 1). In line with this observation, the UV−vis spectral differences in MeOH vs DMF solutions were less pronounced than those in H_2O vs DMF solutions for all of the studied Cr(VI)−thiolato complexes (Figures 3, S4, and S5).

Quantitative formation of a metal complex of a higher coordination number by reversible addition of a solvent ligand to a precursor complex is uncommon, unlike for substitution of a ligand with a solvent molecule, where the complex−solvent adducts can form as unstable intermediates.[52] For instance, reversible additions of H_2O or alcohol molecules have been observed in a series of carbonyl complexes of Mo(0) or W(0), and one such complex, $[W^0(CO)_3\{P(iPr_3)\}_2(OH_2)]$, has been characterized by X-ray crystallography.[53] Similar adduct formation with neutral O- or N-donor ligands is known for oxo complexes of Cr(V)[54] or Os(VIII);[55] these adducts act as intermediates in redox catalysis.[54,55] There have been no previous examples of structurally characterized Cr(VI) complexes with H_2O or ROH ligands, except for a five-coordinate peroxo complex, $[CrO(O_2)_2(OH_2)]$ (the structure has been proposed on the basis of the stopped-flow XAS studies of the Cr(VI) + H_2O_2 reaction in acidic aqueous solutions).[47] The current study again demonstrates the power of XAS in determination of the structures of unstable metal complexes in solutions.[2,21,31,42,56] Application of a statistical approach (Tables 3, 4, S5, and S7)[37] allows more definitive determination of coordination

(48) Van Den Bergen, A.; Colton, R.; Percy, M.; West, B. O. *Inorg. Chem.* **1993**, *32*, 3408−3411.
(49) Stewart, I. I.; Horlick, G. *J. Anal. At. Spectrom.* **1996**, *11*, 1203−1214.
(50) Madhusudanan, K. P.; Katti, S. B.; Vijayalakshmi, R.; Nair, B. U. *J. Mass Spectrom.* **1999**, *34*, 880−884.
(51) Larkworthy, L. F.; Nolan, K. B.; O'Brien, P. In *Comprehensive Coordination Chemistry*; Wilkinson, G., Gillard, R. D., McCleverty, J. A., Eds.; Pergamon Press: Oxford, U.K., 1987; Vol. 3, pp 699−969 and references therein.
(52) Tobe, M. L. In *Comprehensive Coordination Chemistry*; Wilkinson, G., Gillard, R. D., McCleverty, J. A., Eds.; Pergamon Press: Oxford, U.K., 1987; Vol. 1, pp 281−330.
(53) Kubas, G. J.; Burns, C. J.; Khalsa, G. R. K.; Van Der Sluys, L. S.; Kiss, G.; Hoff, C. D. *Organometallics* **1992**, *11*, 3390−3404.
(54) (a) Srinivasan, K.; Kochi, J. K. *Inorg. Chem.* **1985**, *24*, 4671−4679. (b) Samsel, E. G.; Srinivasan, K.; Kochi, J. K. *J. Am. Chem. Soc.* **1985**, *107*, 7606−7617.
(55) Lay, P. A.; Harman, W. D. *Adv. Inorg. Chem.* **1991**, *37*, 219−379 and references therein.
(56) Levina, A.; Lay, P. A.; Foran, G. J. *J. Chem. Soc., Chem. Commun.* **1999**, 2339−2340.

numbers from XAFS data analysis, which is generally a difficult task, particularly for the complexes containing both strongly scattering S-donors and more weakly scattering O/N-donors.[57]

Comparison of the XAS results for sample 6 (Table 1) with those of the ESMS and kinetic studies (Figure 2) shows that $[CrO_3(SR^3)(OH_2)]^-$ is the only relatively stable intermediate Cr species formed during the reduction of Cr(VI) to Cr(III) by excess glutathione in weakly acidic aqueous solutions. Assignment of this intermediate as a Cr(IV) species on the basis of dynamic magnetic susceptibility measurements[15,16] probably suffered from the difficulties in distinguishing between Cr(IV) (d^2) species and mixtures of Cr(VI) (d^0) and Cr(III) (d^3) species in such measurements.

Recently,[20] $[CrO_3(SR^3)]^-$ species were observed by ESMS as the only detectable Cr intermediate during the reduction of Cr(VI) to Cr(III) by glutathione in neutral aqueous media at relatively low concentrations of the reagents ($[Cr(VI)]_0 = 5.0$ mM, $[R^3SH]_0 = 20$ mM, pH 7.4). Since the UV−vis spectra of the Cr(VI)−R^3SH species in acidic and neutral aqueous media (pH 2.9 or 7.4) were practically identical (Figure 4a), it is likely that $[CrO_3(SR^3)(OH_2)]^-$ is also formed during the reduction of Cr(VI) with R^3SH under physiological conditions. The range of R^3SH concentrations used in the kinetic studies (5.0−20 mM, Figure 4 and Table S4) was close to typical intracellular concentrations of this reductant (5−10 mM).[3] Unfortunately, XAS studies of Cr(VI)−thiolato complexes formed during the reactions of Cr(VI) with glutathione and other biological thiols in neutral aqueous solutions are very difficult, as such complexes exist as minor components of mixtures containing $[CrO_4]^{2-}$ and Cr(III) species (Figure 4b).

The absence of UV−vis spectroscopic evidence for deprotonation of the $[CrO_3(SR^3)(OH_2)]^-$ complex at pH 7.4 (Figure 4) can be explained by the rapid decomposition of the deprotonated species ($[CrO_3(SR^3)(OH)]^{2-}$) with the release of R^3SH and the formation of $[CrO_4]^{2-}$ (Scheme 2a). This suggestion is supported by the rapid formation of $[CrO_4]^{2-}$ from the Cr(VI)−R^1SH complex in alkaline aqueous solutions (see the Results). Similarly, the Cr(VI)−R^3SH complex, generated at pH 2.9 (condition 6 in Table 1), rapidly decomposed with the formation of $[CrO_4]^{2-}$ (determined by UV−vis spectroscopy) when added to aqueous buffer solutions at pH 7.4.[58]

Thus, the addition of an aqua ligand to Cr(VI)−thiolato complexes is likely to contribute to the low stability of such complexes in aqueous solutions (particularly at pH ≥ 7), in comparison with the solutions in aprotic solvents,[11] where the less reactive $[CrO_3(SR)]^-$ species are dominant (Scheme 2a). Formation and reactivity of $[CrO_3(SR^3)(OH_2)]^-$ (not $[CrO_3(SR^3)]^-$, as thought before)[10,11] and of similar complexes with other biological thiols have to be taken into account when the roles of Cr(VI)−thiolato complexes in DNA and protein damage are considered.[1,2]

Scheme 2. Proposed Equilibria Involving Cr(VI)−Oxo and Cr(VI)−Thiolato Complexes in Aqueous Solutions (a), Compared with That Involved in Forming a V(V)−Thiolato Complex Bound to the Active Site of PTP (b)[59]

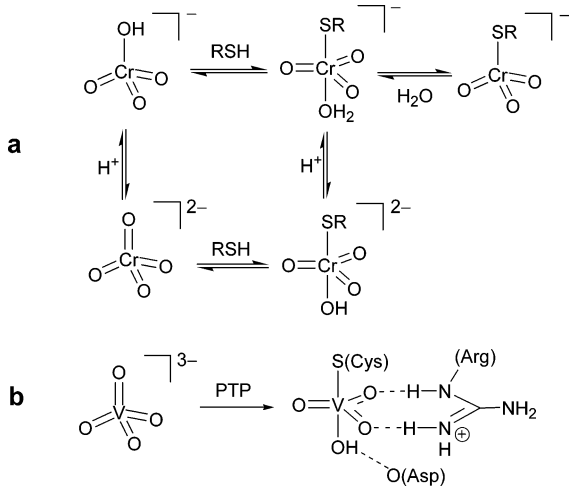

A potentially important biological implication of the formation of five-coordinate Cr(VI)−thiolato complexes in aqueous solutions is revealed by comparison with the chemistry of isoelectronic V(V) species. The tetrahedral vanadate ion binds to active sites of protein tyrosine phosphatases (PTPs; containing a highly conserved Cys-$(X)_5$Arg motif, where X is any amino acid) with the formation of a five-coordinate V(V)−thiolato complex, which is stabilized by a network of H-bonds (Scheme 2b, determined by X-ray crystallography).[59] Such complexes are responsible for the well-known role of vanadate as an inhibitor of PTPs, since a stable five-coordinate V(V) center acts as a mimic of a transition state of phosphate in these enzymes.[59] Similarly, formation of five-coordinate Cr(VI)−PTP complexes may lead to inhibition of PTPs in Cr(VI)-treated cells (in agreement with the experimentally observed increased levels of tyrosine phosphorylation in such cells),[60] and provide a chemical basis for the similarity in biological activities of V(V) and Cr(VI), including their actions as insulin mimetics.[2] Thus, structural characterization of Cr(VI)−thiolato complexes in aqueous solutions provides important insights into potential biological roles of these species.

Acknowledgment. Financial support of this work was provided by Australian Research Council (ARC) Large and Discovery Grants and an ARC Professorial Fellowship (to P.A.L.), and by ARC Infrastructure grants for ESMS and stopped-flow equipment and the 10-element Ge detector at the ANBF. The EPR instrumentation was funded by ARC LIEF and Wellcome Trust Equipment grants. This work was supported by the Access to Major Facilities Program funded

(57) Clark-Baldwin, K.; Tierney, D. L.; Govindaswamy, N.; Gruff, E. S.; Kim, C.; Berg, J.; Koch, S. A.; Penner-Hahn, J. E. *J. Am. Chem. Soc.* **1998**, *120*, 8401−8409.
(58) Levina, A.; Ludwig, C.; Lay, P. A. *J. Inorg. Biochem.* **2003**, *96*, 177.
(59) (a) Zhang, M.; Zhou, M.; Van Etten, R. L.; Stauffacher, C. V. *Biochemistry* **1997**, *36*, 15−23. (b) Zhang, Z.-Y.; Wang, Y.; Wu, L.; Fauman, E. B.; Stuckey, J. A.; Schubert, H. L.; Saper, M. A.; Dixon, J. E. *Biochemistry* **1994**, *33*, 15266−15270.
(60) (a) Yurkow, E. J.; Kim, G. *Mol. Pharmacol.* **1995**, *47*, 686−695. (b) Qian, Y.; Jiang, B.-H.; Flynn, D. C.; Leonard, S. S.; Wang, S.; Zhang, Z.; Ye, J.; Chen, F.; Wang, L.; Shi, X. *Mol. Cell. Biochem.* **2001**, *222*, 199−204.

by the Department of Industry, Science and Resources and managed by the Australian Nuclear Science and Technology Organisation. X-ray absorption spectroscopy was performed partially at the ANBF with support from the Australian Synchrotron Research Program, which is funded by the Commonwealth of Australia under the Major National Research Facilities program, and partially at the Stanford Synchrotron Radiation Laboratory, a national user facility operated by Stanford University on behalf of the U.S. Department of Energy, Office of Basic Energy Sciences. The SSRL Structural Molecular Biology Program is supported by the Department of Energy, Office of Biological and Environmental Research, and by the National Institutes of Health, National Center for Research Resources, Biomedical Technology Program. We thank Dr. Peter Barnard (University of Sydney) and Drs. Garry Foran and James Hester for assistance with data collection at the ANBF, Drs. Britt Hedman, Matthew Latimer, and Alison Soo Hoo for assistance at the SSRL, and Drs. Alexei Kuzmin and Juris Purans (Solid State Physics Institute, University of Latvia) for helpful discussions on XAS data processing.

Supporting Information Available: Figures showing (i) FTIR spectra of $(Ph_4As)[CrO_3(SR^1)]$, R^1SH, and $(Ph_4As)Cl$, (ii) negative-ion mode ESMS spectra of the reaction mixtures used for XAS, and experimental and simulated signals of the Cr(VI)−thiolato complexes, (iii) UV−vis spectra of the Cr(VI)−R^1SH complex in mixed-solvent systems, (iv) solvent dependencies of UV−vis spectra of the Cr(VI)−R^2SH complex, (v) details of XANES spectra, and (vi) experimental and calculated (SS models) XAFS and FT XAFS spectra and tables showing (i) experimental settings of XAS, (ii) assignment of major ESMS signals, (iii) UV−vis spectral parameters of Cr(VI)−thiolato complexes in various solvents, (iv) results of kinetic analyses of the Cr(VI) + R^3SH reactions, and (v) details of the conditions and results of SS and MS XAFS analyses. This material is available free of charge via the Internet at http://pubs.acs.org.

IC034901V